Quarterly Journal of the Royal Meteorological Society *Q. J. R. Meteorol. Soc.* 141: 182–194, January 2015 A DOI:10.1002/qj.2348

Assimilation of oceanographic observations with estimates of vertical background-error covariances by a Bayesian hierarchical model

Srdjan Dobricic,[a]* Christopher K. Wikle,[b] Ralph F. Milliff,[c] Nadia Pinardi[d] and L. Mark Berliner[e]

[a]*Centro EuroMediterraneo sui Cambiamenti Climatici, Bologna, Italy*
[b]*Department of Statistics, University of Missouri, Columbia, USA*
[c]*CIRES, University of Colorado, Boulder, USA*
[d]*Department of Physics and Astronomy, University of Bologna, Italy*
[e]*Department of Statistics, Ohio State University, Columbus, USA*

*Correspondence to: S. Dobricic, JRC, Via E. Fermi 2749, 21027 Ispra (VA), Italy.
E-mail: srdan.dobricic@jrc.ec.europa.eu

A new method to estimate the vertical part of the background-error covariance matrix for an ocean variational data assimilation system is presented and tested in the Mediterranean operational daily analysis system. The operational, seasonally varying error covariances are compared with high-frequency estimates from a Bayesian Hierarchical Model (BHM) which estimates distributions for the vertical error covariances from two data-stage inputs: model anomalies and differences between model background and observations, i.e. so-called misfits. It is found that the posterior mean BHM-error covariance estimates that vary on 5-day time-scales reduce the misfits root mean square of the analysis vertical profiles of temperature and salinity by 10–20% versus analyses arising from covariances that vary on seasonal time-scales or those from the BHM given only model anomalies as data stage inputs.

Key Words: Bayesian hierarhical model; data assimilation; oceanography

Received 07 October 2013; Revised 05 February 2014; Accepted 11 February 2014; Published online in Wiley Online Library 27 March 2014

1. Introduction

The assimilation of observations in operational oceanography must be performed rapidly in order to produce a forecast in real time. Further, such assimilation must be based on models that are able to resolve the oceanographic processes of interest at the finest affordable spatial and temporal scales and it should assimilate all data, both satellite and *in situ*.

These specific operational conditions require the use of data assimilation schemes with a number of assumptions and simplifications in order to combine, in near-real time, a large number of observations with high-resolution oceanographic models that have large computational requirements. For example, the global systems providing forecasts with the highest horizontal resolution by MetOffice, Mercator, US Navy and BlueLink apply either the three-dimensional variational (3D-Var) data assimilation schemes (Cummings and Smedstad, 2013; Blockley *et al.*, 2014), or simplified versions of the Singular Evolutive Extended Kalman (SEEK) filter and the Ensemble Kalman Filter with climatological estimates of background-error covariances (Brasseur and Verron, 2006; Oke *et al.*, 2007). As another example, the daily oceanographic analysis cycle of the Mediterranean Forecasting System (MFS), assimilating all available satellite and *in situ* observations with a model having the horizontal resolution of approximately 6 km and 70 levels (Dobricic *et al.*, 2007; Pinardi and Coppini, 2010) is accomplished in 2 min, while 5 min are required to run a 1-day-long forecast on a machine with relatively few processors. This computational efficiency is achieved by applying a 3D-Var scheme named 'OceanVar' (Dobricic and Pinardi, 2008) which simplifies the time and space variability of the error covariance matrix.

The OceanVar scheme splits the estimate of background-error covariance into slowly and rapidly varying parts. The slowly evolving part contains the vertical error covariances in temperature (T) and salinity (S), since it is thought that the physical process time-scales underlying these vertical covariances are typically longer than the daily data assimilation cycle. These vertical covariances are computed seasonally from model simulation T, S anomalies and vary between horizontal regions with different dynamical characteristics. The rapidly evolving part of the error covariances are considered only for errors related to sea level and the horizontal velocities (Dobricic and Pinardi, 2008).

An important background error in the MFS system appears to be associated with the vertical representation of the seasonal and main thermocline variability (e.g. Dobricic *et al.*, 2005; Adani *et al.*, 2011; Pinardi *et al.*, 2011). For the Mediterranean Sea, the maximum errors concentrate in the first 50 m of the water column, where the seasonal thermocline forms, and in the intermediate layers (200–400 m), where advection of intermediate salty waters from the eastern Mediterranean occurs. The water formation processes, both in the mixed, intermediate and deep layers, have high-frequency components, from a few hours to days, that are difficult to model using only low-frequency seasonal variability in the vertical error covariance of T and S. Thus, it is important for data assimilation to better represent the vertical error variability while maintaining computational efficiency, adhering to operational time constraints.

There are several well-known methods that can account for the model dynamics in the data assimilation error covariances. In oceanography they include the four-dimensional variational data assimilation (e.g. Weaver *et al.*, 2003; Di Lorenzo *et al.*, 2007; Moore *et al.*, 2011), the ensemble Kalman filter (Evensen, 1994) and methods based on the reduced-order approximations of background-error covariances (e.g. Lermusiaux and Robinson, 1999; Brasseur and Verron, 2006). While with the linear assumption all these methods provide dynamically consistent estimates of the background-error covariances with the actual dynamical evolution of the model state, they also require a large number of model integrations. Therefore, their applicability in the operational environment where the analysis must be available in real time is possible only with a certain reduction of the model resolution and/or the model domain. As already mentioned, this may be avoided in the variational approach by 3D-Var and in the optimal interpolation approach by simplified SEEK or Ensemble Kalman Filter in which climatological estimates approximate background-error covariances.

Alternatively, we consider hierarchical Bayeisan methods for data assimilation. The use of Bayesian methods in the atmospheric and ocean sciences goes back quite some time (e.g. Epstein, 1962; Olsen, 1975). More critically for this application, Berliner (1996) described a simple hierarchical Bayesian paradigm for modelling physical processes, which has since proven useful across a variety of atmospheric and ocean processes (e.g. the recent summaries in Cressie and Wikle, 2011; Wikle *et al.*, 2013). Wikle and Berliner (2007) discussed the plausibility of using this hierarchical Bayesian paradigm in the context of a traditional data assimilation analysis, extending the purely Bayesian connections to data assimilation as discussed in Lorenc (1986). One way to implement such a hierarchical Bayesian data assimilation approach is to model the covariance structure associated with the background- and/or model-error covariances, and if possible, to do so in a time-varying fashion. Hierarchical Bayesian models for covariance matrices have been shown in the statistical literature to be facilitated by various forms of matrix decompositions (e.g. Daniels and Purahmadi, 2002; Chen and Dunson, 2003). Such methods have not been used in the context of data assimilation.

In this study we propose a method for estimating the temporal evolution in the background-error covariances by adopting the Bayesian Hierarchical Model (BHM) approach (e.g. Berliner, 1996; Cressie and Wikle, 2011) and extending the statistical methodology of Chen and Dunson (2003). We seek to develop an error covariance BHM that allows for resolving temporal evolution, on 5-day time-scales, of the vertical error covariance matrix. In particular, the hierarchical Bayesian framework allows for borrowing strength from data time series, and can easily accommodate multiple data sources. In our case, we will use data both from T and S anomalies from a reanalysis dataset and actual differences between observations and model background state estimates, so-called misfits. The latter contain the high-frequency variability in the vertical error covariances discussed above. The BHM will use these two data stages to estimate the high-frequency vertical error covariance variability for OceanVar. We refer to this model as 'BHM-error covariances' (for Bayesian Hierarchical Model for Error Covariances) and we will show its impact on the MFS analysis quality.

The article is organized as follows: section 2 describes the data assimilation and the error covariance formalism, section 3 the model and the numerical experiments, while sections 4 and 5 discuss the results of assimilation experiments using the observations of only one Argo profile as well as a complete, satellite and *in situ*, data assimilation case. A discussion section concludes the article.

2. BHM for background-error covariances

2.1. *Data assimilation scheme and error covariance matrices*

OceanVar computes the ocean analysis by minimizing the following cost function:

$$J = \frac{1}{2}\delta\mathbf{x}^{\mathrm{T}}\mathbf{B}^{-1}\delta\mathbf{x} + \frac{1}{2}\left(\mathbf{d} - \mathbf{H}\delta\mathbf{x}\right)^{\mathrm{T}}\mathbf{R}^{-1}\left(\mathbf{d} - \mathbf{H}\delta\mathbf{x}\right), \qquad (1)$$

where $\delta\mathbf{x} = \mathbf{x} - \mathbf{x}_{\mathrm{b}}$ is the perturbation in the model space around the background state $\mathbf{x}_{\mathrm{b}}$, $\mathbf{B}$ and $\mathbf{R}$ are background- and observational-error covariance matrices, $\mathbf{H}$ is the linearized form of the observational operator $H()$, and $\mathbf{d} = \mathbf{y} - H(\mathbf{x}_{\mathrm{b}})$ is the misfit between observations $\mathbf{y}$ and background estimates. All model field state variable perturbations make up $\delta\mathbf{x}$, i.e. temperature, salinity, horizontal velocities and sea surface height. The minimization is achieved by making perturbations in a control space. The mapping of perturbations into a control space is given by:

$$\delta\mathbf{x} = \mathbf{V}\mathbf{v}, \qquad (2)$$

where $\mathbf{v}$ is the perturbation in the control space and $\mathbf{V}$ is the mapping operator representing the square root of the background-error covariance matrix, i.e.

$$\mathbf{B} = \mathbf{V}\mathbf{V}^{\mathrm{T}}. \qquad (3)$$

In Dobricic and Pinardi (2008) $\mathbf{V}$ is defined as a sequence of linear operators:

$$\mathbf{V} = \mathbf{V}_{\mathrm{F}}\mathbf{V}_{\mathrm{H}}\mathbf{V}_{t_{\mathrm{S}}}. \qquad (4)$$

In Eq. (4), $\mathbf{V}_{\mathrm{F}}$ represents a sequence of linear operators that describe the filtering and velocity part of background-error covariances, not important for this study, and $\mathbf{V}_{\mathrm{H}}$ represents horizontal error covariances for temperature and salinity that are modelled by a Gaussian correlation function depending on the radial distance. The operator $\mathbf{V}_{t_{\mathrm{S}}}$ represents vertical error covariances of T and S at the seasonal time-scale, t_{S}. In the MFS operational system, $\mathbf{V}_{t_{\mathrm{S}}}$ is composed of 20 vertical Empirical Orthogonal Functions (EOFs) computed for each season from anomalies relative to the seasonal mean of a long model simulation (Dobricic *et al.*, 2007).

2.2. *Time-varying vertical covariance modelling with a BHM*

Following Berliner *et al.* (2003) and Cressie and Wikle (2011), we organize the BHM error covariance implementation into components leading to a posterior distribution for vertical T and S error covariances. The posterior distribution arises according to Bayes Theorem as the convolution of probability distributions for: (i) data stage inputs; (ii) process model stage formulations; and (iii) the parameters from each (data and process). These components are described in greater detail in this section. The Appendix briefly discusses the procedure for estimating the posterior distribution given these components. A particular innovation in this application is the inclusion of misfit information from Argo profiles as a data stage input. These data support the higher temporal frequency that is the goal for the vertical error covariance model for T and S.

We use the BHM to substitute the $\mathbf{V}_{t_{\mathrm{S}}}$ in Eq. (4) with an operator containing faster time-scales, of the order of a few days. Let

$$\mathbf{B}_{V_t} = \mathbf{V}_t\mathbf{V}_t{}^{\mathrm{T}}, \qquad (5)$$

be the vertical error covariance matrix component of Eq. (3), where the subscript t represents the shorter time-scale temporal evolution and $\mathbf{V}_t$ the faster time-scale operator to be constructed with BHM.

Two forms of input data are used in the BHM. The first are the daily anomalies in each model point, $\mathbf{x}_{ti}$, of the actual model state with respect to the 2003–2008 monthly mean mean values, indicated by the overbar with T:

$$\mathbf{q}_{ti} = \mathbf{x}_{ti} - \overline{\mathbf{x}_{ti}}^{\mathrm{T}}. \tag{6}$$

The second are the misfits defined as differences between observations $\mathbf{y}_{ti}$ and background estimates with their monthly mean value again subtracted:

$$\mathbf{d}_{ti} = \mathbf{y}_{ti} - H(\mathbf{x}_{ti}) - \overline{\{\mathbf{y}_{ti} - H(\mathbf{x}_{ti})\}}^{\mathrm{T}}, \tag{7}$$

where $H()$ is the observational operator, considered here to be a three-dimensional linear interpolator. Vector $\mathbf{x}_{ti}$ contains vertical profiles of temperature followed by vertical profiles of salinity for each horizontal point i, while vector $\mathbf{y}_{ti}$ contains in the same sequence temperature and salinity profiles by Argo floats.

2.2.1. BHM: Data model

The BHM data stage incorporates the assumption that the two data sources, Eqs (8) and (9), follow Gaussian (normal) distributions conditioned on the true temperature and salinity background errors, represented by the $2n$-dimensional vector $\mathbf{e}_t$, where 2 is the number of variables (temperature and salinity) and n is the number of depth levels, i.e.

$$\mathbf{q}_t|\mathbf{e}_t \sim N(\mathbf{H}_{q_t}\mathbf{e}_t,\ \boldsymbol{\Sigma}_{q_t}), \tag{8}$$

and

$$\mathbf{d}_t|\mathbf{e}_t \sim N(\mathbf{H}_{d_t}\mathbf{e}_t,\ \boldsymbol{\Sigma}_{d_t}), \tag{9}$$

where $\mathbf{H}_{q_t}$ and $\mathbf{H}_{d_t}$ are $m_{q_t} \times 2n$ and $m_{d_t} \times 2n$ dimensional incidence (zero/one) matrices accounting for potential missing observations at time t, where m_{qt} and m_{dt} are the number of levels for which we have data at time t for q and d respectively, and $\boldsymbol{\Sigma}_{q_t}$ and $\boldsymbol{\Sigma}_{d_t}$ are the associated m_{q_t} and m_{d_t}-dimensional measurement-error covariance matrices defined as

$$\boldsymbol{\Sigma}_{i,t} = \begin{pmatrix} \sigma^2_{i,tT} & 0 \\ 0 & \sigma^2_{i,tS} \end{pmatrix}, \tag{10}$$

for $i = d, q$. We will specify prior distributions for the variance components in Eq. (10) in the parameter stage (section 2.1.3).

2.2.2. BHM: Process model

In order to reduce the computational cost and filter the computational noise, we assume that the background-error covariance matrix in Eq. (3) can be represented in terms of $2n \times p$ dimensional seasonal EOF vertical error structure functions, $\mathbf{U}_{t_S}$, and the associated p-dimensional faster-varying amplitudes $\boldsymbol{\beta}_t$. The BHM error process model is then given by:

$$\mathbf{e}_t = \mathbf{U}_{t_S}\boldsymbol{\beta}_t + \boldsymbol{\eta}_t, \qquad \eta_t \sim N(0, \tau_t\mathbf{I}), \tag{11}$$

where τ_t is the error variance that accommodates small-scale variability and ensures that the error covariance matrix implied by Eq. (11) is non-singular. The amplitude coefficients

$$\boldsymbol{\beta}_t \approx N(0,\ \boldsymbol{\Lambda}_t\,\boldsymbol{\Gamma}_t\,\boldsymbol{\Gamma}_t^{\mathrm{T}}\boldsymbol{\Lambda}_t) \tag{12}$$

use a modified Cholesky decomposition form for the covariance matrix, where $\boldsymbol{\Lambda}_t$ is a diagonal matrix with elements proportional to the standard deviations of the random variable β_t and $\boldsymbol{\Gamma}_t$ is a lower triangular matrix that is associated with the correlations among the elements of $\boldsymbol{\beta}_t$ (Chen and Dunson, 2003). Implementation of the hierarchical model is facilitated by recognizing that we can write $\mathbf{e}_t$ equivalently as

$$\mathbf{e}_t = \mathbf{U}_{t_S}\boldsymbol{\Lambda}_t\boldsymbol{\Gamma}_t\mathbf{b}_t + \boldsymbol{\eta}_t, \qquad \boldsymbol{\eta}_t \sim N(0, \tau_t\mathbf{I}), \tag{13}$$

which suggests that we can write the time-varying covariance matrix $\mathbf{B}_{Vt} = \mathrm{var}(\mathbf{e}_t)$ in the following form:

$$\mathbf{B}_{Vt} = \mathbf{U}_{t_S}\boldsymbol{\Lambda}_t\,\boldsymbol{\Gamma}_t\,\boldsymbol{\Gamma}_t^{\mathrm{T}}\boldsymbol{\Lambda}_t\,\mathbf{U}_{t_S} + \tau_t\mathbf{I}\,. \tag{14}$$

2.3. BHM: Parameter models

To complete the hierarchical formulation, we must specify distributions for the parameters in the process model Eq. (13). In particular, we specify the elements of the diagonal matrix $\boldsymbol{\Lambda}_t$ and the lower triangular elements of $\boldsymbol{\Gamma}_t$ to follow independent random walk distributions as given in the Appendix. In addition, the data model variance components given in Eq. (14) and the time-varying additive variance component in the same equation are assumed to be inverse-gamma prior distributions (see the Appendix). Estimation is then carried out using Markov Chain Monte Carlo (MCMC) methods as summarized briefly in the Appendix.

2.4. Application of the BHM-error covariance to the MFS data assimilation system

The two data stage vectors, $\mathbf{q}_{it}$ and $\mathbf{d}_{it}$, contain T and S daily values extracted from a Mediterranean reanalysis dataset (Adani *et al.*, 2011) for the period from 2003 to 2008 in the northwestern region of the Mediterranean (Figure 1). This figure shows the two data inputs as anomalies from their monthly means. It is evident that while $\mathbf{q}_{it}$ has a large periodic component for T, corresponding to the variance associated with the formation of the seasonal thermocline in the region, the S components of $\mathbf{q}_{it}$ and $\mathbf{d}_{it}$ for both T and S have a more 'episodic' structure and variance content on time-scales of a few days. This higher-frequency variability corresponds to mixed- and deep-layer water formation events and advections of salinity anomalies. This region contains the Gulf of Lions, which is one of the few global sites of deep convection in the Northern Hemisphere winter. The complicated and wide-ranging seasonal and episodic water mass variability in the Gulf of Lions provides an opportunity for thorough testing of the time-varying error covariance taken from the BHM.

For application in the MFS data assimilation system, we have computed 40 seasonal EOFs, $\mathbf{U}_{t_S}$, for the daily dataset of $\mathbf{q}_{ti}$ from the surface to 1000 m, as done in the operational system Dobricic *et al.* (2007). This corresponds to 46 model levels and thus the data stage input vector has a dimension of 92 with 46 levels for temperature and 46 levels for salinity.

The new high-frequency vertical operator is then obtained by an eigenvalue decomposition of $\mathbf{B}_{Vt}$. This is done by applying the Lanczos algorithm on $\mathbf{B}_{Vt}$ in Eq. (14). Thus, in OceanVar the operator $\mathbf{V}_{vt}$ defined in Eq. (5) becomes:

$$\mathbf{V}_{vt} = \mathbf{S}_{t_S}\mathbf{L}_t, \tag{15}$$

where the columns of $\mathbf{S}_{t_S}$ are eigenvectors and diagonal elements of $\mathbf{L}_t$ contain square roots of eigenvalues of $\mathbf{B}_{Vt}$. It should be noted that the eigenvalue decomposition of $\mathbf{B}_{Vt}$ has different square roots than the lower triangular decomposition defined in Eq. (14). However, the difference is only due to a change in the control space, while in the physical space both definitions of the square root should give the same perturbations of T and S. The decomposition in Eq. (15) is needed in order to optimize the minimization algorithm in OceanVar. By visually comparing the temporally evolved $\mathbf{B}_{Vt}$ with different choices of the data stage period used to determine $\boldsymbol{\beta}_t$ in Eq. (12), we have chosen to update $\mathbf{B}_{Vt}$ every 5 days because any shorter time-scales

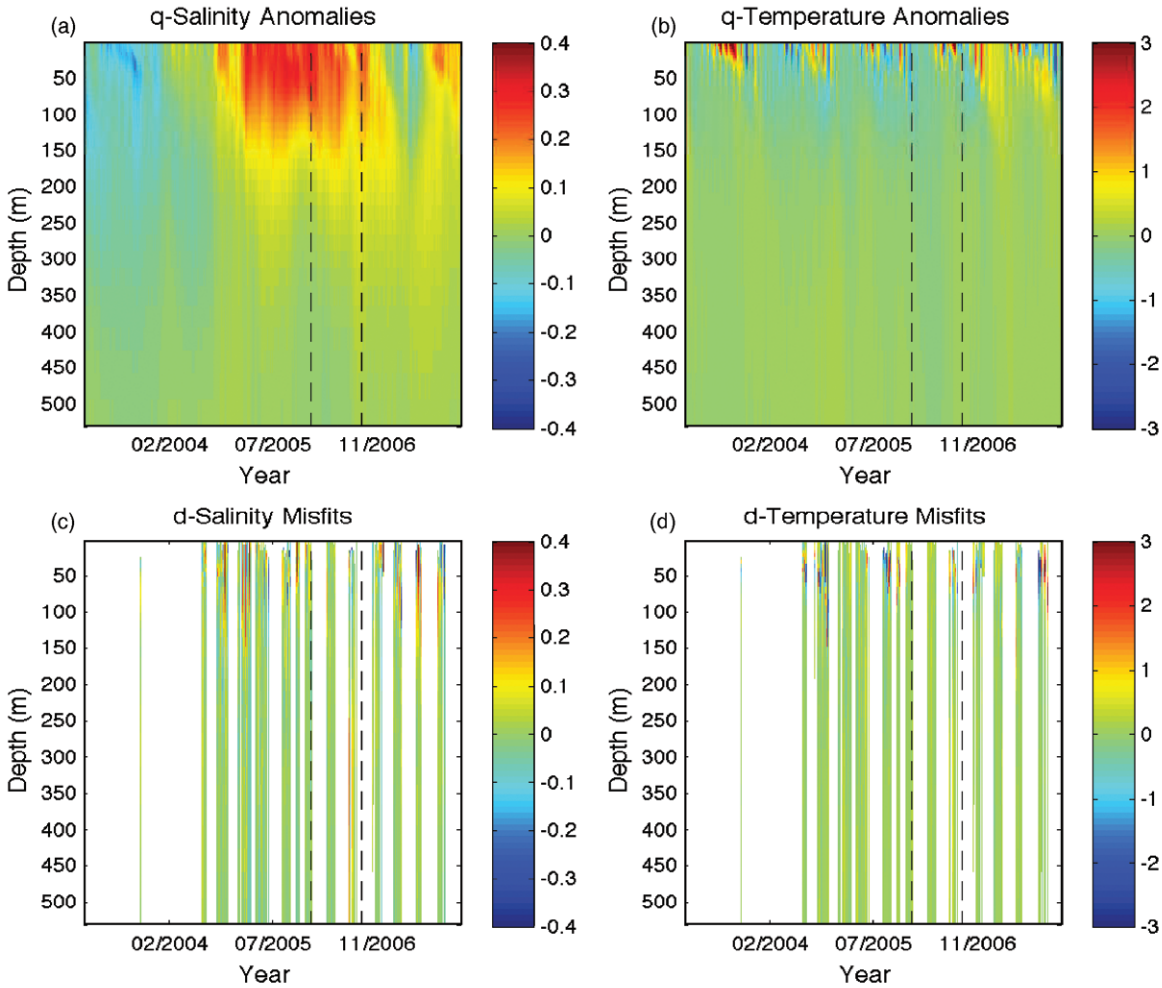

Figure 1. The model (a, b) anomalies and (c, d) misfit profile time series for (a, c) salinity, and (b, d) temperature, averaged over region 3 of the northwestern Mediterranean shown Figure 5(a).

would not have enough misfits to sample the region adequately since Argo observations in the Mediterranean Sea have a 5-day surfacing cycle (Poulain *et al.*, 2007). So this article contrasts the seasonal background vertical-error covariance from the operational system, changing abruptly four times per year, versus $\mathbf{B}_{Vt}$ from BHM-error covariance method wherein variability in error covariances can smoothly resolve temporal scales on the order of 5 days.

Figure 2 shows two examples of how the BHM method changes the estimates of the error covariances. On 10 February 2006 the BHM estimates of $\mathbf{B}_{Vt}$ exhibit variances of background temperature and salinity three times larger than the climatological estimate for winter. The increase in variance is even larger on 10 July 2006 with respect to climatological variances in summer (Figure 2). The latter difference is especially large for the surface temperature. Clearly, the BHM method has increased the covariance, adding information to the seasonal estimates from the variability of model and misfit vertical profiles on particular days.

An interesting feature of temperature error variances on 10 February 2006 is the presence of three local maxima: at the surface, level 20 ($\sim$ 125 m) and level 40 ($\sim$ 615 m). The last two are positioned quite deep and may reflect the uncertainties due to the weak vertical stratification and enhanced deep mixing. Eventually the fact that the background temperature errors at levels 20 and 40 are negatively correlated may indicate the possible mixing of temperature between these two levels. That is, the negative change of temperature at level 20 could be correlated with the positive change of temperature at level 40 as a product of mixing that does not significantly change the temperature between these two levels, but expands the thickness of this well-mixed layer.

It can be further seen in Figure 2 that in summer both seasonal and BHM estimates show the largest error covariances in the temperature mixed layer in the top 10 levels (down to $\sim$ 40 m depth), while the winter covariances are more equally spread towards deeper layers and between temperature and salinity. This general agreement between climatological/seasonal and BHM covariances reflects the dynamical processes of stratification due to the heating of surface layers in summer and weak stratification due to the surface cooling in winter.

Figure 3 shows the vertical covariances in temperature and salinity errors with temperature errors at level 10 ($\sim$ 40 m). Once again, the major difference between the climatological and BHM estimate is the large increase in the covariance magnitudes in the BHM estimate. The increase is especially evident in the top layers. On 10 July 2006 the BHM estimate shows an opposite sign in the temperature covariance at the surface with respect to level 10. This feature may indicate the process of the vertical mixing which may enhance or reduce the vertical stratification. The climatological estimate has the same-signed temperature error covariance, indicating an overall heating or cooling process near the surface layers. Isolated mixing events, occurring over a few days, would be missing from the seasonal background-error covariances.

In Figures 2 and 3, the BHM error covariance matrix used is the mean of the posterior distribution for B_{Vt}. While it can be argued that the posterior mean B is a sensible choice to examine the impact of faster time-scale vertical error covariances in T and S, it does not fully exploit the power of BHM.

The variance of background-error covariances matrices estimated by the BHM is shown in Figure 4. In the EOF space scaled by the layer thickness and standard deviations of temperature and salinity anomalies (Dobricic *et al.*, 2005, give

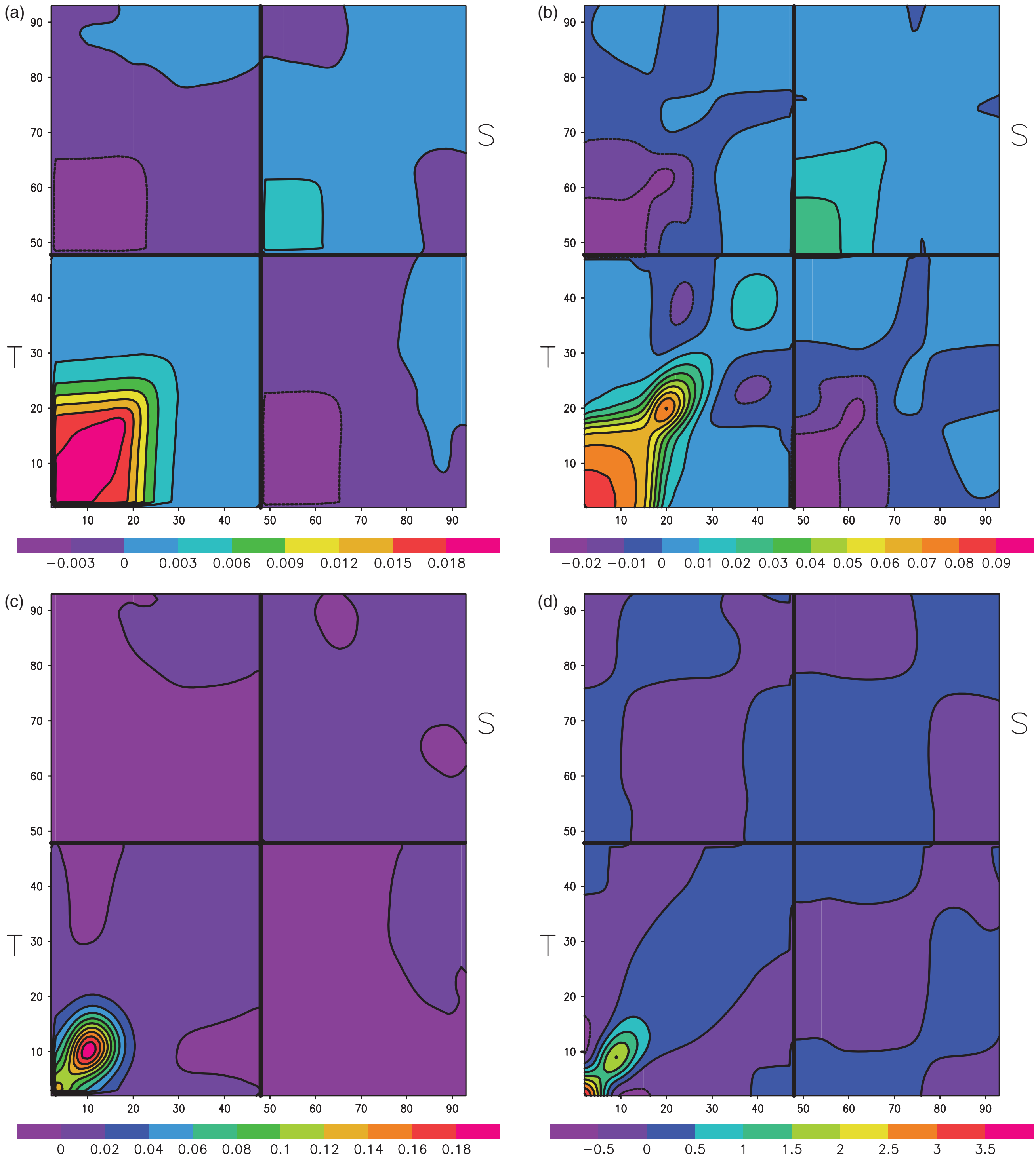

Figure 2. (a) shows the operational $V_{Vt_S} V_{Vt_S}^{\mathrm{T}}$ vertical error-covariance matrix in winter for the region of the northwestern Mediterranean, (b) shows the BHM B_{Vt} estimate on 10 February 2006. (c) shows the operational $V_{Vt_S} V_{Vt_S}^{\mathrm{T}}$ vertical error covariance for summer, and (d) its BHM B_{Vt} estimate on 10 July 2006. The numbers on the axis refer to the model levels where the first 46 values represent temperature and the second 46 values represent the salinity levels. Matrix blocks representing covariances of T and S, and their cross-covariances are divided by a cross over the matrix. T and S covariance blocks are labelled on the axes. Dimensions are physical (°C for temperature and psu for salinity). Note that each panel has a different colour bar.

the description of the computation of EOFs), the temperature variance is concentrated at levels 15–25 (75–200 m) in winter and at level 5 (15 m) in summer. Salinity variance has the maximum at the surface in winter and at level 20 (125 m) in summer. In the physical space the temperature variance in winter and in summer becomes large near the surface, and it dominates the variance of BHM estimates of B_{Vt}.

In later work, we will consider implications to be drawn from the posterior distribution shapes and changes from prior specifications for covariances and parameters of the BHM. As a second step toward this end, we compare below analyses obtained from the posterior mean covariances with those from a single, randomly selected, realization of the covariance from the posterior distribution for B_{Vt}.

3. Numerical experiments

3.1. *Description of MFS system*

MFS consists of an Ocean General Circulation Model (OGCM) implemented in the whole Mediterranean Sea (Oddo *et al.*, 2009) and the OceanVar data assimilation scheme (Dobricic and Pinardi, 2008). The OGCM is based on the NEMO code (Madec, 2008) and it has a regular latitude–longitude grid with

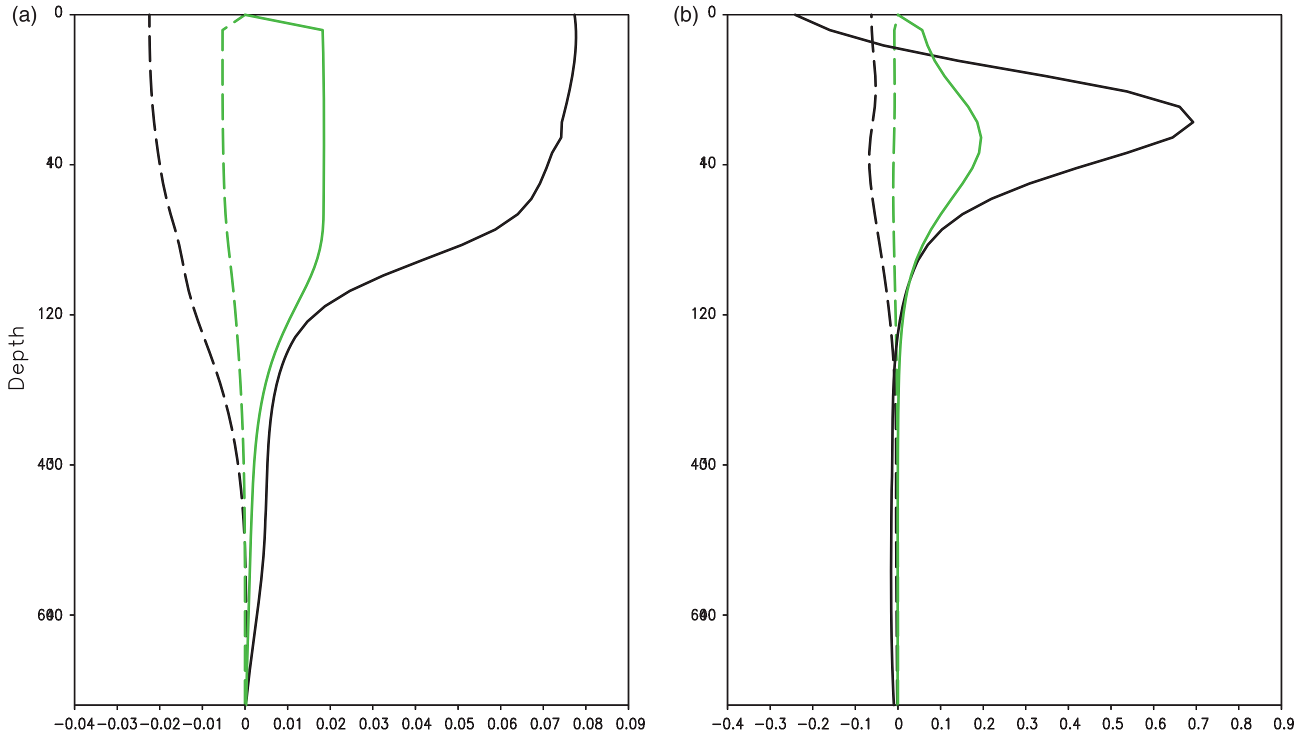

Figure 3. Covariances with temperature at level 10 (40 m) for temperature and salinity for region 3 of the northwestern Mediterranean: (a) operational values (green) for winter and BHM estimates (black) on 10 February 2006, (b) operational values (green) for summer, and the BHM estimates (black) on 10 July 2006. Full lines represent temperature and dashed lines salinity at 46 model levels. Units are physical (°C for temperature and psu for salinity).

a resolution of 1/16°; i.e. 7 km in the meridional and 5 km in the zonal directions. The model has 72 levels with a level thickness of 3 m at the surface, smoothly increasing to 300 m for the deepest level (5000 m). The model extends far into the Atlantic Ocean in order to freely simulate the exchange through the Gibraltar Strait. It uses an implicit free surface scheme and utilizes the European Centre for Medium-range Forecasts (ECMWF) operational atmospheric analyses for the calculation of atmospheric fluxes. The Mediterranean part of the horizontal model domain is shown in Figure 5.

The OceanVar data scheme assimilates, with a daily cycle, *in situ* observations of temperature and salinity profiles by Argo drifters, temperature profiles from expendable bathythermographs (XBTs) and satellite observations of Sea Level Anomaly (SLA), as described in Dobricic *et al.* (2007).

3.2. *Experimental set-up*

The performance of the BHM estimate of the background vertical-error covariances is compared with the climatological estimate in the period from 1 January to 1 September 2006, using the mean covariance estimate from the BHM posterior distribution. During this period, two Argo floats continuously occupied positions in the northwestern part of the Mediterranean Sea, where the BHM estimated distributions for new background-error covariances on 5-day time-scales (Figure 4). During this 8-month period, the ARGO floats covered different vertical stratification regimes. This period spanned the well-mixed and often vertically unstable conditions leading to deep convection in late winter, to the strongly stratified surface layers in summer.

Six experiments were performed as summarized in Table 1. Two control experiments (CNTRL and CNTRL-A) use the seasonal estimate of vertical background-error covariances. Two experiments (BHM-Q and BHM-A-Q) use the BHM estimates that include only the T and S anomalies, i.e. the q data stage in Eq. (8). The remaining two experiments (BHM-QD and BHM-A-QD) use BHM estimates that also include the misfits in Eq. (9). The first set of three experiments (CNTRL, BHM-Q and BHM-QD) assimilate only *in situ* temperature and salinity profiles from a single Argo float (the blue circles in Figure 5) which occupied the region of interest in the northwestern Mediterranean. This set of experiments was used to evaluate how each error covariance estimate is able to resolve the vertical structure of temperature and salinity corrections without any impact from other observations. The second set of three experiments (CNTRL-A, BHM-A-Q and BHM-A-QD) assimilate all *in situ* and SLA observations in the Mediterranean, but the estimates of the BHM background vertical-error covariances are done only in the northwestern region.

3.3. *Experiments with the assimilation of a single Argo float*

The impact of the different estimates of background-error covariances is illustrated in Figure 6. It shows the observed, background and analyzed profiles of temperature and salinity for the first assimilation step in the 8-month period for the first three experiments where only a single Argo float was used. We focus on this particular time step because the background profiles for the control and BHM experiments are identical and the differences in the analysis are solely due to different error covariance estimates. As shown in Figure 6, the temperature and salinity analyses with and without BHM are significantly different. The difference is especially evident at depths between 200 and 350 m where the BHM analysis forms a local minimum in both temperature and salinity, while the control analysis has the minimum only in salinity. Minima in temperature and salinity at the depths between 200 and 350 m indicate the presence of cold, low-salinity waters intruding into the offshore regions. The salinity and temperature minima are positioned just above local maxima in temperature and salinity which indicate the presence of the Levantine Intermediate Water advected from the east.

The differences in the analyses were even larger later in the period, showing the cumulative effect of using the BHM vertical error covariances. Figure 7 shows how, even at the later time, the BHM analysis produces different vertical profiles of temperature and salinity. Although in this case it is not possible to subtract the impact of background fields that differ in each experiment and the comparison is not independent, once again in the BHM case, the analyzed temperature and salinity are closer to the observations in places with large vertical gradients.

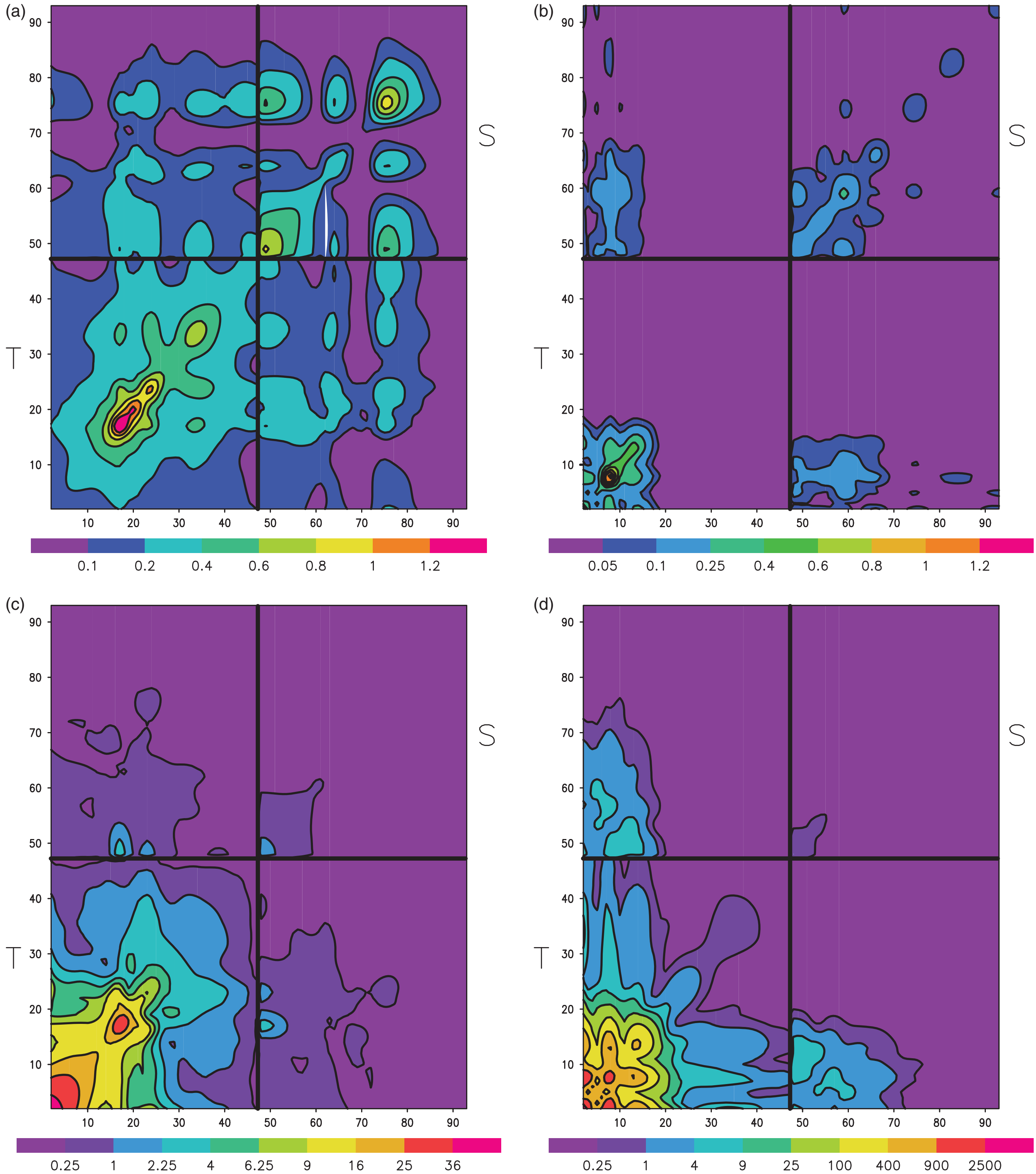

Figure 4. The variance of B_{Vt} is shown in (a, b) scaled and (c, d) physical spaces on (a,c) 10 February 2006, and (b, d) 10 July 2006. The numbers on the axis refer to the model levels where the first 46 values represent temperature and the second 46 values represent the salinity levels. Matrix blocks representing covariances of T and S, and their cross-covariances are divided by a cross over the matrix. T and S covariance blocks are labelled on the axes. The scaled space is non-dimensional, and in the physical space the dimensions are $^{\circ}C^2$ for temperature and psu^2 for salinity. Note that each panel has a different colourbar and the line spacing is not constant.

Table 1. List of the six experiments used for the evaluation of the impact of BHM background-error covariances.

Experiment name	Short description	Observational dataset used
CNTRL	Climatological EOFs	One ARGO profile asimilated
BHM-QD	BHM EOFs with Q and D	One ARGO profile assimilated
BHM-Q	BHM EOFs only with Q	One ARGO profile assimilated
CNTRL-A	Climatological EOFs	All SLA and ARGO assimilated
BHM-A-QD	BHM EOFs with Q and D	All SLA and ARGO assimilated
BHM-A-Q	BHM EOFs only with Q	All SLA and ARGO assimilated

Both temperature and salinity profiles at depths between 50 and 150 m are smoother and closer to observations in the BHM analysis.

The accuracy of the analysis is evaluated by calculating the RMS of misfits for the ARGO data. As the sampling frequency of ARGO is 5 days, we argue that the advection is not strong enough to propagate away the information from the previous analysis, so that the RMS of misfits gives us an almost independent data evaluation of the analysis quality. The assumption that the information from the previous analysis is not advected far from the float may be partly justified by the fact that the float is advected

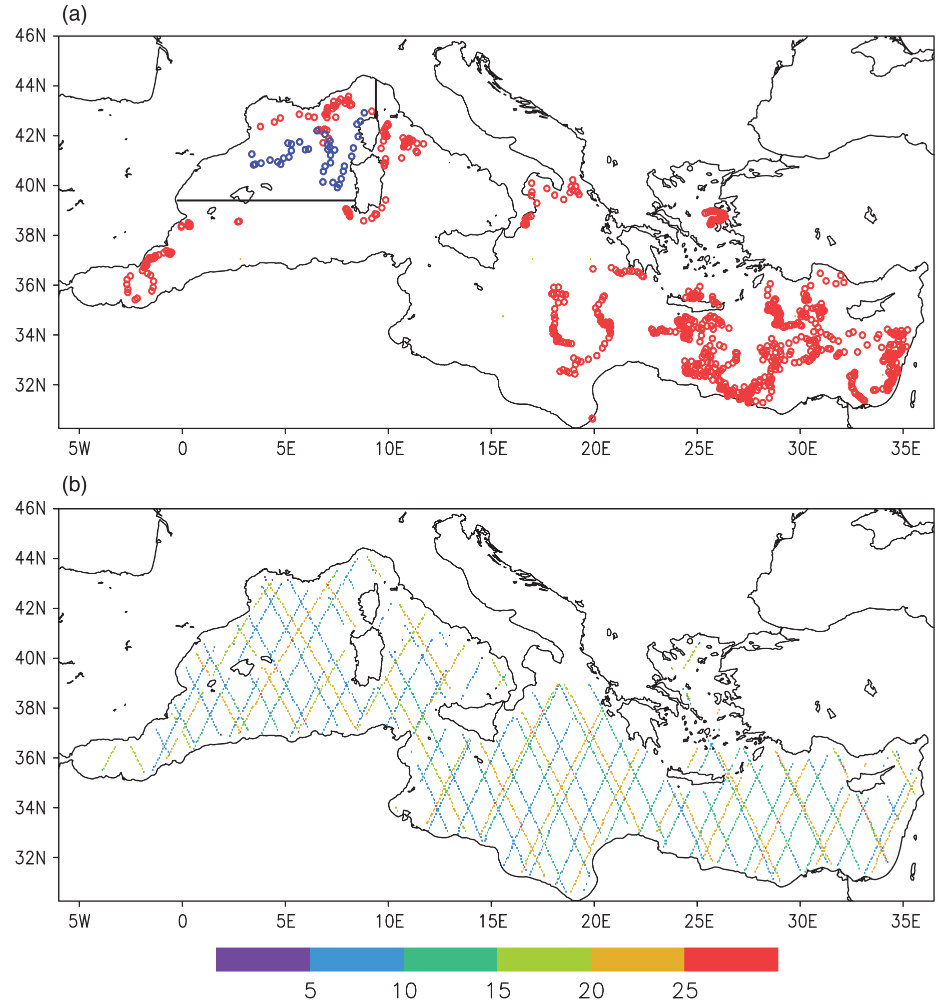

Figure 5. Positions of (a) Argo floats and (b) SLA tracks for the period January–August 2006. Blue dots in (a) indicate the positions of the single Argo float used for the assimilation in experiments CNTRL, BHM-Q and BHM-QD, and red dots indicate positions of other floats. The straight lines denote region 3 in which the BHM error covariances are calculated. In (b) colours indicate the number of SLA observations during the experiment.

at the depth of 350 m where velocities are typically smaller than in the upper layers. It should be further noted that in 5 days, the errors from inaccurate model equations and the atmospheric forcing could become the dominant factor in the RMS error of misfits.

Figure 8 shows the RMS of misfits in successive 5-day periods averaged over the 8 months, and Figure 9 shows the relative difference between the RMS for BHM-Q and BHM-QD and the RMS of CNTRL. With respect to CNTRL, temperature misfits are reduced in both BHM-Q and BHM-QD. BHM-QD shows the overall best performance, mainly by reducing the maximum error in both temperature and salinity at 50 m by about 20%. The salinity analysis in experiment BHM-QD is also most accurate in the deep layers where the relative improvement also reaches 20%.

The mean of temperature misfits was negligible except at the surface where all experiments underestimated the observed temperatures by 0.2 °C, while the mean of salinity misfits was negligible except at the layer below the surface where it reached 0.08 psu (not shown).

3.4. *Experiments with assimilation of all observations*

In the second group of experiments, all observations of temperature and salinity and satellite altimetry are assimilated in the entire Mediterranean basin. The only difference between experiments CNTRL-A, BHM-A-Q, and BHM-A-QD is the different BHM vertical background-error covariances used in the northwestern region. Contrary to the previous set of experiments with a single Argo float sampling the vertical T and S profiles, now satellite SLA observations are also assimilated. In this case, the vertical background-error covariances are used by the data assimilation scheme to extrapolate the information from the sea-level misfits onto increments of temperature and salinity throughout the water column. This is an even more important test for the BHM estimate of vertical background-error covariances because the extrapolated vertical profiles of temperature and salinity could be different from the *in situ* profiles near Argo float positions and this would generate inconsistencies if the vertical error covariances are not appropriate for the specific time.

Figures 10 and 11 show the RMS of temperature and salinity misfits for CNTRL-A, BHM-A-Q and BHM-A-QD. In particular, this time BHM-A-Q exhibits larger RMS than CNTRL-A in the top 300 m of the water column, while BHM-A-QD exhibits consistently lower RMS of misfits throughout the water column. The RMS of salinity misfits is reduced up to 20% at 100 m for the BHM-A-QD with respect to CNTRL-A. It is interesting to notice that the relative improvement of the RMS of temperature and salinity misfits is comparable and sometimes even larger than the improvement obtained with a very similar model set-up and the sequential variational (SVAR) data assimilation scheme (Dobricic, 2013), which dynamically estimates the evolution of background-error covariances.

At the surface, the RMS of temperature misfits is slightly increased, while the RMS of salinity misfits is slightly decreased. Once again, as in experiments with the single float, it can be argued that the difference between RMS of misfits near the surface can also be attributed to errors in the atmospheric forcing. The RMS of misfits calculated with respect to Argo observations and SLA outside the northwestern region (not shown) were practically indistinguishable between experiments. Apparently the effect of the BHM vertical error covariances is only local to

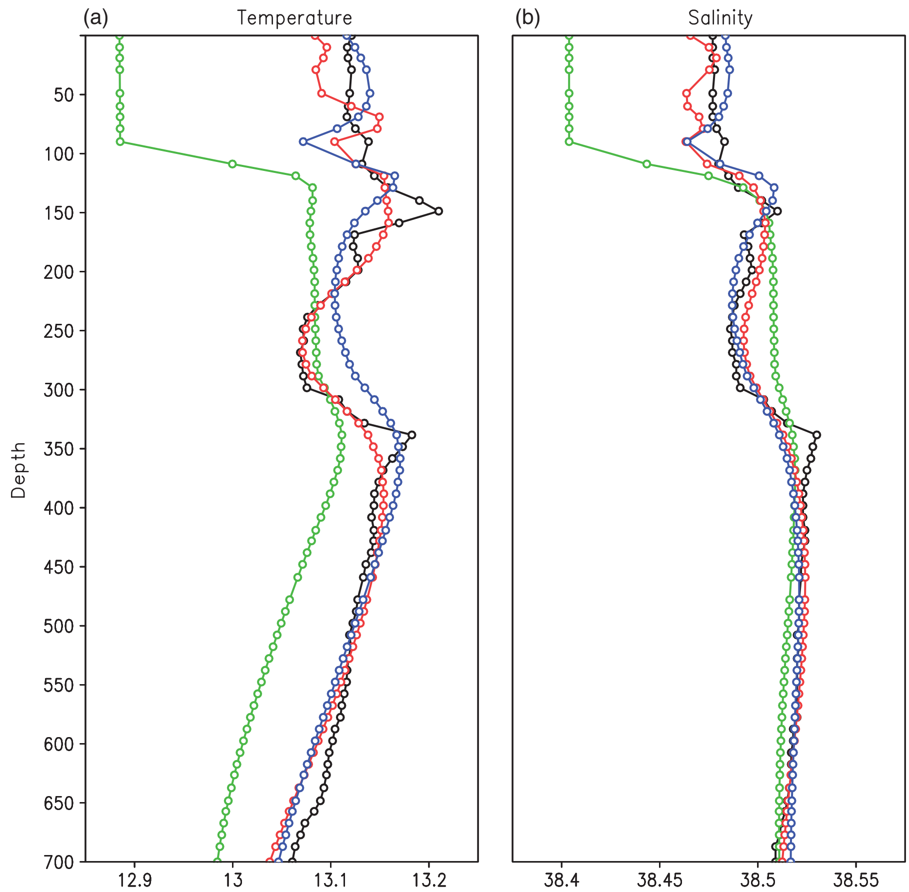

Figure 6. Profiles of background (green), observation (black), CNTRL analysis (blue) and BHM-QD analyses (red) for (a) temperature and (b) salinity. Analyses are made on 2 January 2006 by using the first ARGO profile in the northwestern Mediterranean. The dots indicate observations.

the region where it is applied. Also, it appears that the vertical error structures in BHM were not significantly different in order to reduce the uncertainty of the sea-level field even within the region of interest. The RMS of SLA misfits (not shown) are approximately the same in all three experiments. It could be that the horizontal formulation of background-error covariances is more important for the sea level uncertainty, or that simply the improvement seen in temperature and salinity fields is not detected by SLA observations.

In experiments with all observations, the mean of temperature and salinity misfits was very similar to the one obtained in the experiment with a single float. It was negligible in the deeper layers and near the surface reached 0.2 °C for temperature and 0.08 psu (not shown). We may assume that, in all experiments, misfits were random, except close to the surface where in addition to the initial state error they could have been significantly influenced by model and atmospheric forcing errors.

As noted earlier, the analyses to this point are based on the posterior mean vertical error covariance from the BHM. We expect that individual realizations from the posterior will yield different analyses and different values for misfit RMS. As a first test of this assumption, we have performed an additional experiment with all available observations and a randomly chosen realisation from the posterior distribution of BHM parameters. The RMS of temperature and salinity misfits is shown in Figures 10 and 11 by the dashed line. In this experiment the RMS of temperature misfits is significantly reduced in the top 100 m with respect to all other experiments, but it is larger than the one by the CNTRL-A below. In the top 300 m, the experiemnt also produces the largest RMS of salinity misfits.

The RMS misfit reductions due to a randomly selected realization from the posterior distribution for the vertical error covariance are not as favorable as they were for the posterior mean case. We have yet to fully explore and summarize the information content of the full posterior distribution in this context.

4. Discussion

In this study we implemented a BHM approach to estimate the high-frequency, temporally variable part of the background vertical temperature and salinity error covariances in Eq. (14). In the traditional MFS system, only seasonally varying vertical EOFs are used from the analysis of model T and S anomalies (i.e. the 'q' data). The BHM-error covariance method instead allows us to combine two sources of information, the model anomalies and the misfits (i.e. the 'd' data). These are the data stage inputs to the BHM which then determine time-varying error covariances and variances, on 5-day time-scales, from a re-analysis dataset from 01 January to 1 September 2006 using seasonal EOFs calculated from a longer period, from 1997 to 2007. The posterior mean BHM-error covariance matrices introduce background-error covariance features that are more consistent with the current model dynamics and misfits.

The method is applied in the MFS operational set-up to assimilate different kinds of data. The impact of the new BHM-error covariances is tested in two sets of numerical experiments: single Argo and all data experiments. Sensitivity of the BHM error covariance method to the two data stage inputs is tested by restricting (or not) the inclusion of misfit data together with the model T, S anomalies. In the first set of experiments, we evaluated the improvements due to the BHM method when the innovation is due to temperature and salinity profiles from a single Argo float, in a single sub-region of interest. In the second set of experiments, the impact is evaluated in a more realistic ocean forecast configuration where the background temperature and salinity error covariances extrapolate the information from satellite SLA observations in combination with *in situ* observations from several ARGO floats.

The experiments presented here evaluated the impact by calculating the RMS of temperature and salinity misfits in the region where the new background-error covariances were

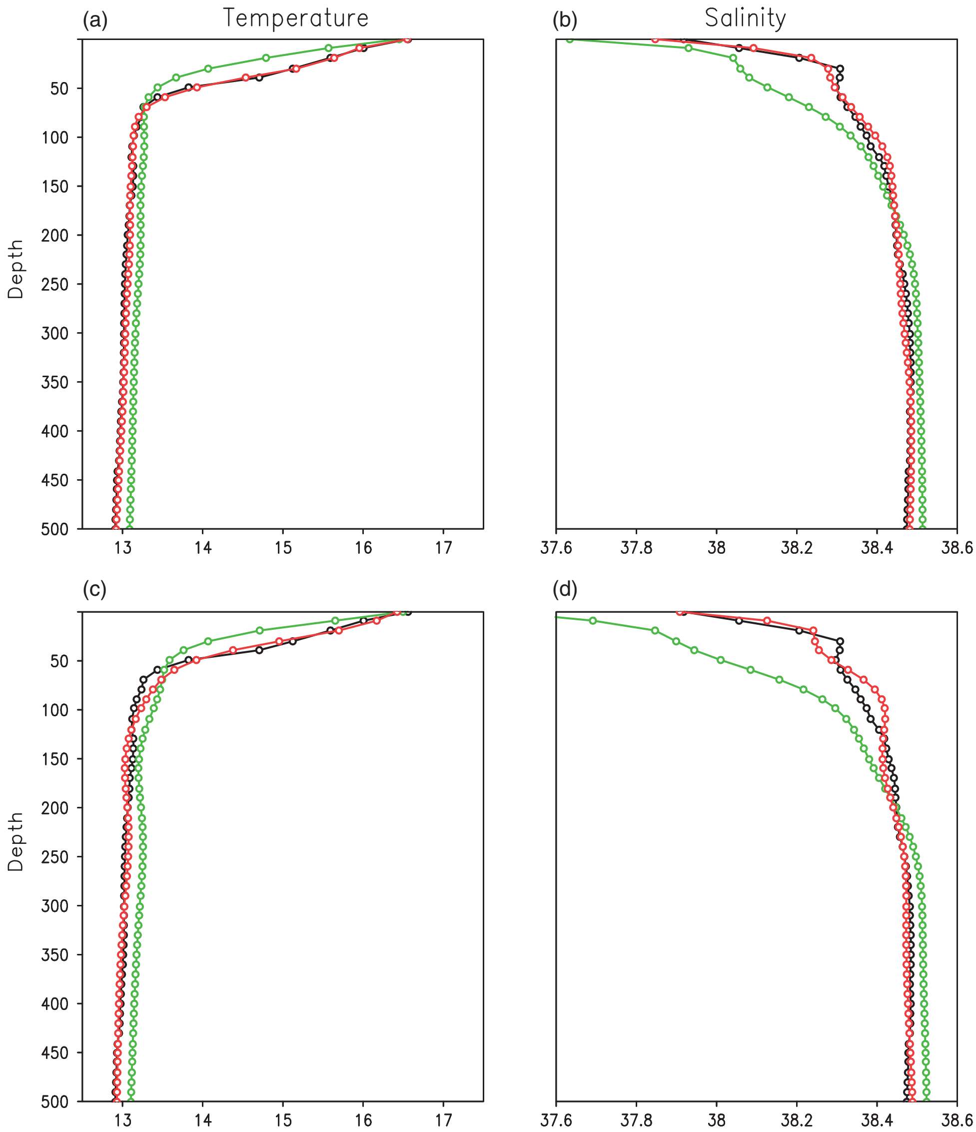

Figure 7. Profiles of background (green), observation (black) and analysis (red) for (a, c) temperature and (b, d) salinity. Analyses are made on 7 May 2006 for (a, b) experiment BHM-QD and (c, d) experiment CNTRL. The dots indicate denote observations.

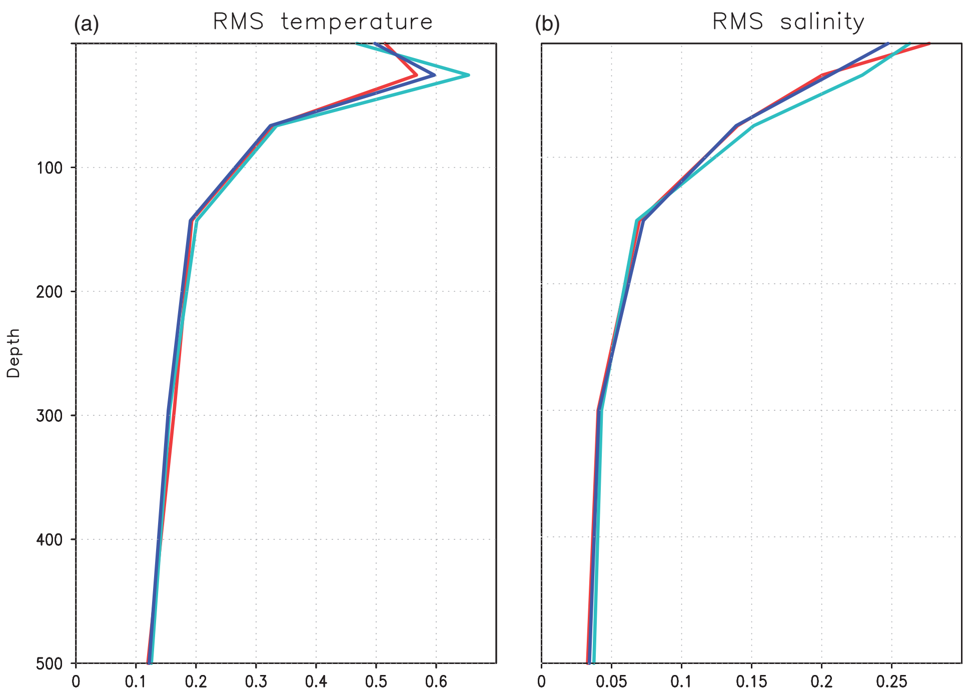

Figure 8. The RMS of (a) temperature (°C) and (b) salinity (psu) for experiments assimilating a single Argo float, from the CNTRL experiment (cyan), the BHM-Q experiment (blue) and the BHM-QD experiment (red).

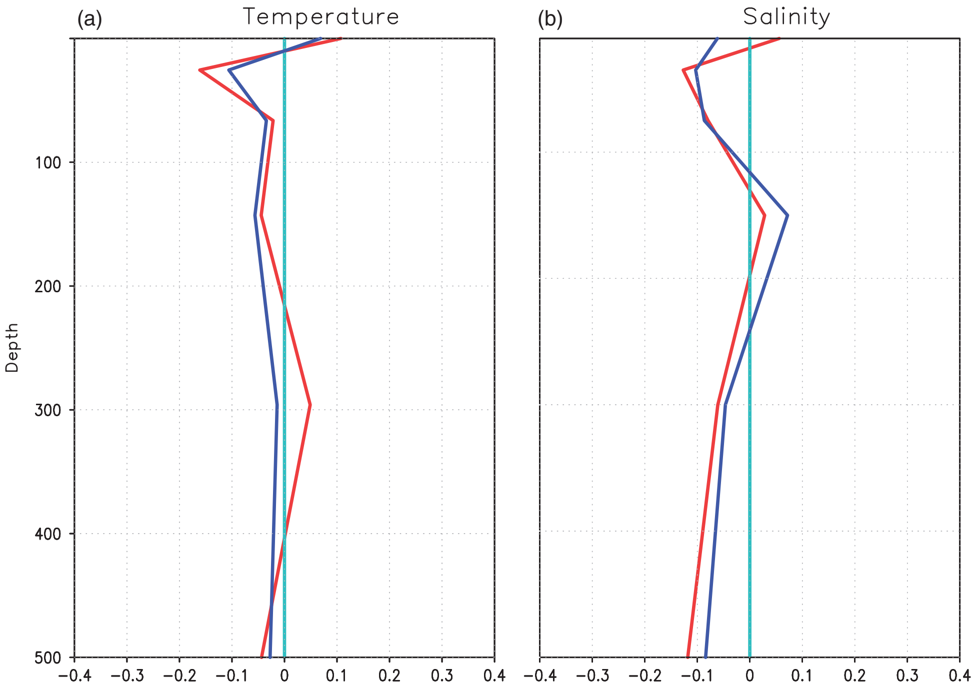

Figure 9. As Figure 8, but for the relative difference between the RMS of misfits in each experiment and the RMS of misfits in the control experiment, for CNTRL (cyan), BHM-Q (blue) and BHM-QD (red).

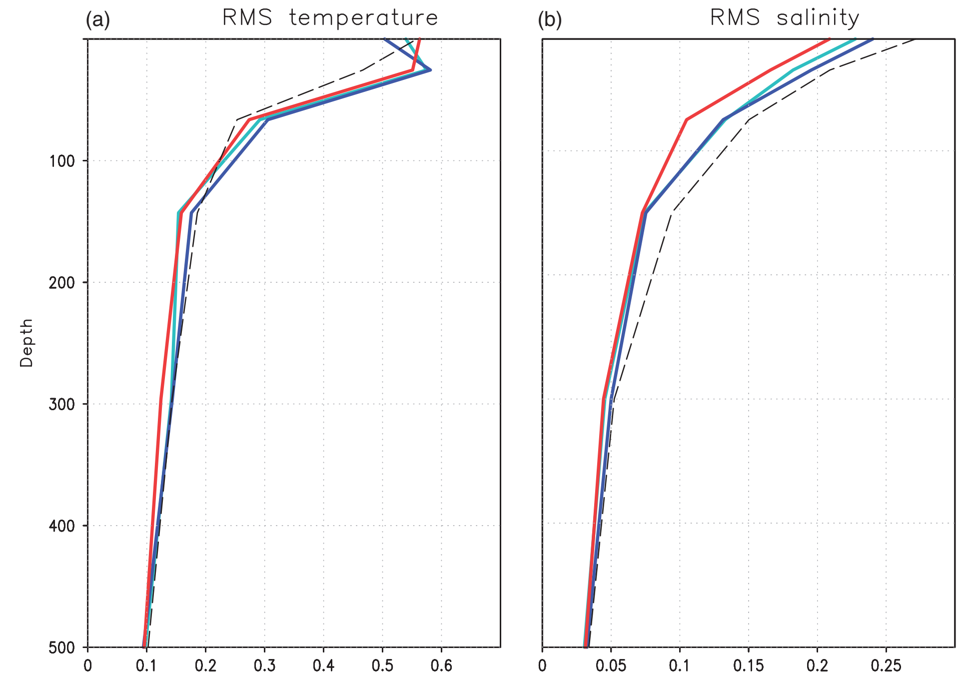

Figure 10. The RMS of misfits for (a) temperature (°C) and (b) salinity (psu) for experiments assimilating all observations, from CNTRL-A (cyan), BHM-A-Q (blue) and BHM-A-QD (red). The black dashed line shows the RMS of misfits for the experiment with the randomly chosen realization of BHM.

applied. Both sets of experiments showed that the BHM method improved the accuracy of the analyses with respect to the original seasonal background-error covariances method. However, the improvement was not significant when the BHM method used only the data stage with model anomalies. On the other hand, when the misfits were used as additional data stage inputs, the RMS of temperature and salinity misfits was significantly reduced for all parameters over the 8-month study period.

This result may be surprising, because it is generally believed that only model anomaly estimates should lead to more accurate background-error covariances with respect to seasonal/climatological estimates (e.g. Di Lorenzo *et al.*, 2007). The reason for this result may be due to the fact that the BHM does not estimate the covariances from a full set of perturbed model states, but splits the error covariance into horizontal and vertical modes, the latter valid for relatively large regions. Therefore, the addition of the information from misfits can significantly improve the performance of the BHM method and produce more accurate analyses than the application of model climatological estimates only.

It should be noted that the idea to combine the current information from misfits in order to update the estimates of background-error covariances has been applied in several other studies. For example, Wang *et al.* (2008) increased the variance of the ensemble anomalies by scaling it with averaged squares of misfits. Desroziers *et al.* (2005) modified the covariances by using the diagnostics of the cost function. Contrary to these methods, the BHM method includes the misfit additional information by using the least feasible number of assumptions regarding the relationship between observational and background errors by applying a general Bayesian theory and Monte Carlo sampling.

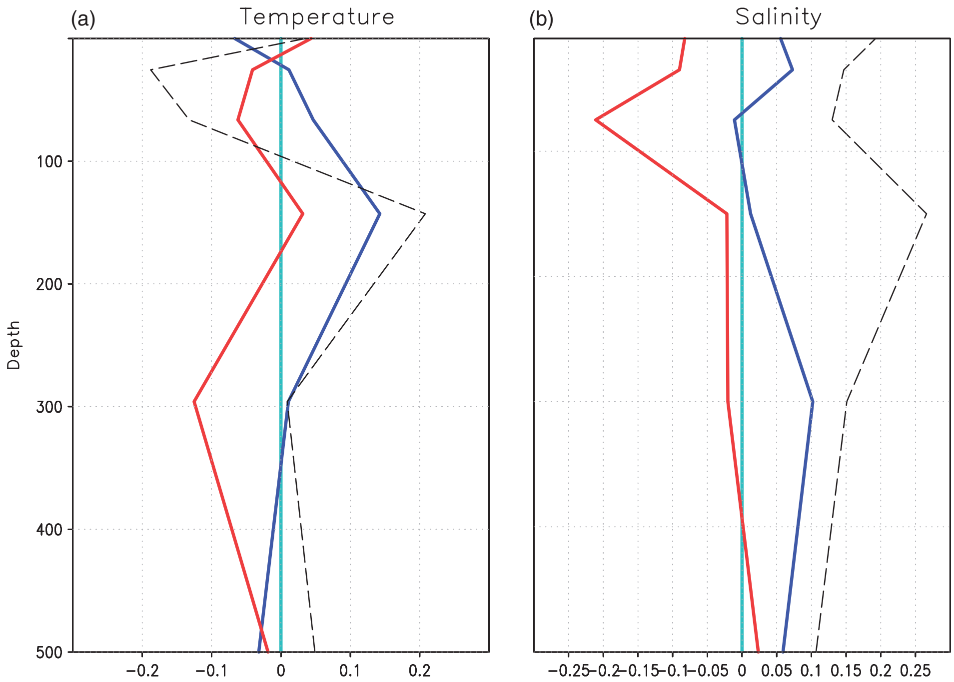

Figure 11. As Figure 10, but for the relative difference between the RMS of misfits in each experiment and the RMS of misfits in the control experiment.

It is interesting to note that, by combining the climatological estimates (for the EOFs) with the current model estimates of background-error covariances, the BHM method has some similarity to the hybrid method applied in Hamill and Snyder (2000), Etherton and Bishop (2004) or Wang *et al.* (2007). However, one of the major differences between these two methods is that in the hybrid method the weights given to the climatological and model estimates are arbitrary, while in the BHM they arise directly from the computations based on Bayes' theorem.

There are several possible future extensions of the BHM method for estimating background-error covariances. One possibility may be to apply it with an ensemble of analyses and forecasts in a framework similar to the hybrid analysis method. Another possibility is to refine the vertical error process model in a way similar to the one given in Behringer and Leetmaa (1998). Furthermore, one could sample realizations of the BHM-error covariances instead of using only the posterior mean. In particular, this extension could evaluate a major assumption made in this study that the mean of the posterior distribution is the most appropriate estimate for background-error covariances. In all future extensions, the BHM will be an excellent framework for defining in a theoretically consistent way the covariances of errors between background parameters.

Acknowledgements

We thank ONR projects N00014-05-C-0198 (RFM) and N00014-05-10337 (CKW). In particular we thank Dr M. Fiadeiro for his steadfast interest and support. We thank Dr Gregg Jacobs and Prof. Andrew M. Moore for useful discussions. SD was supported from the Italian Ministry of Education, University and Research and the Ministry for Environment, Land and Sea under the project GEMINA. NP was supported by the project MyOcean and ONR Global funding during her visits to CORA in 2005 and 2008.

Appendix

Estimation of time-varying vertical error covariances by Markov chain Monte Carlo

Section 2 outlines the BHM for time-varying covariance matrices. A summary of the data model, process models, and parameter models for this BHM is given in Table A1. Note that the hyperparameters for the distributions given in the table were chosen to be as non-informative of prior distributions as possible, with the notable exception that we seek to minimize the importance of the additive variance component τ_t and so put a fairly tight prior on it with a fairly small mean. In addition, we have specified tighter priors for the measurement error variance components, with more uncertainty represented in the salinity measurements than the temperature measurements.

As is standard now in the analysis of BHMs, we utilize a Markov Chain Monte Carlo (MCMC) procedure to obtain samples from the ergodic distribution corresponding to the posterior distribution of all random quantities in the model (process and parameters) given the observations (e.g. overviews in Robert and Casella, 2004; Cressie and Wikle, 2011). We note that the choice of the process and parameter distributions here simplify the implementation of the MCMC in that all parameters can be updated through Gibbs sampling steps with the exception of the λ_t parameters, which must be sampled using

Table A1. Hierarchical model summary.

Data models

$\mathbf{d}_t|\mathbf{e}_t \sim N(\mathbf{H}_{d_t}\mathbf{e}_t,\ \mathbf{\Sigma}_{d_t}),\ t = 1,\ldots,T$
$\mathbf{q}_t|\mathbf{e}_t \sim N(\mathbf{H}_{q_t}\mathbf{e}_t,\ \mathbf{\Sigma}_{q_t}),\ t = 1,\ldots,T$

Process model

$\mathbf{e}_t|\mathbf{\Lambda}_t, \mathbf{\Gamma}_t, \mathbf{b}_t, \tau_t \sim N(\mathbf{U}_{t_S}\mathbf{\Lambda}_t\mathbf{\Gamma}_t\mathbf{b}_t,\ \tau_t\mathbf{I}),\ t = 1,\ldots,T$

Parameter models (I)

for $t = 1,\ldots,T$
$\mathbf{b}_t \sim N(\mathbf{0},\ \mathbf{I})$
$\gamma_t(i)\,|\,\sigma^2_\gamma(i) \sim N\{\gamma_{t-1}(i), \sigma^2_\gamma(i)\},\ i = 1,\ldots,n_g$
$\log\{\lambda_t(i)\}|\,\sigma^2_\lambda(i) \sim N\big[\log\{\lambda_t(i)\}, \sigma^2_\lambda(i)\big],\ i=1,\ldots,p$

Parameter models (II)

$\tau_t \sim IG(2.0, 2000)^*,\ t = 1,\ldots,T$
$\gamma_0(i) \sim N(0, 10),\ i = 1,\ldots,n_g$
$\log\{\lambda_t(i)\} \sim N(0, 10),\ i = 1,\ldots,p$
$\sigma^2_\gamma(i) \sim IG(2.01, 0.99),\ i = 1,\ldots,n_g$
$\sigma^2_\lambda(i) \sim IG(2.10, 0.09),\ i = 1,\ldots,p$
$\sigma^2_{d,T} \sim IG(2.0, 10),$
$\sigma^2_{d,S} \sim IG(2.0, 20),$
$\sigma^2_{q,T} \sim IG(2.0, 10),$
$\sigma^2_{q,S} \sim IG(2.0, 20).$

*$IG(a,b)$ corresponds to an inverse gamma distribution with mean $(1/b)/(a\text{-}1)$ and variance $(1/b)^2/((a\text{-}1)^2(a\text{-}2))$.

a Metropolis–Hastings step. The MCMC was run for 20 000 iterations beyond a 2000 iteration burn-in.

References

Adani M, Dobricic S, Pinardi N. 2011. Quality assessment of a 1985–2007 Mediterranean Sea reanalysis. *J. Atmos. Oceanic Technol.* **28**: 569–589, doi: 10.1175/2010JTECHO798.1

Behringer DW, Ji M, Leetmaa A. 1998. An improved coupled model for ENSO prediction and implications for ocean initialization. Part I: The ocean data assimilation system. *Mon. Weather Rev.* **126**: 1013–1021.

Berliner LM. 1996. Hierarchical Bayesian time-series models. *Maximum Entropy and Bayesian Methods*, Hanson KM, Silver RN. (eds.): 15–27. Kluwer: Dordrecht, Netherlands.

Berliner LM, Milliff RF, Wikle CK. 2003. Bayesian hierarchical modelling of air–sea interaction. *J. Geophys. Res.* **108**: 3104, doi: 10.1029/2002JC001413.

Blockley EW, Martin MJ, McLaren AJ, Ryan AG, Waters J, Lea DJ, Mirouze I, Peterson KA, Sellar A, Storkey D. 2014. Recent development of the Met Office operational ocean forecasting system: An overview and assessment of the new Global FOAM forecasts. *Geosci. Model Dev. Discuss.* **6**: 6219–6278, doi: 10.5194/gmdd-6-6219-2013.

Brasseur P, Verron J. 2006. The SEEK filter method for data assimilation in oceanography: A synthesis. *Ocean Dyn.* **56**: 650–661, doi: 10.1007/s10236-006-0080-3.

Chen Z, Dunson DB. 2003. Random effects selection in linear mixed models. *Biometrics* **59**: 762–769.

Cressie N, Wikle CK. 2011. *Statistics for Spatio-Temporal Data*. John Wiley & Sons: Hoboken, NJ.

Cummings JA, Smedstad OM. 2013. Variational data assimilation for the global ocean. In *Data Assimilation for Atmospheric, Oceanic and Hydrologic Applications*, Park SK, Xu L. (eds.): 303–343. Springer: Berlin and Heidelberg, Germany, doi: 10.1007/978-3-642-35088-7_13.

Daniels MJ, Purahmadi M. 2002. Bayesian analysis of covariance matrices and dynamic models for longitudinal data. *Biometrika* **89**: 553–566.

Desroziers G, Berre L, Chapnik B, Poli P. 2005. Diagnosis of observation, background- and analysis-error statistics in observation space. *Q. J. R. Meteorol. Soc.* **131**: 3385–3396.

Di Lorenzo E, Moore AM, Arango HG, Cornuelle BD, Miller AJ, Powell B, Chua BS, Bennett AF. 2007. Weak and strong constraint data assimilation in the inverse Regional Ocean Modelling System (ROMS): Development and application for a baroclinic coastal upwelling. *Ocean Modell.* **16**: 160–187.

Dobricic S. 2013. An application of sequential variational method without tangent linear and adjoint model integrations. *Mon. Weather Rev.* **141**: 307–323, doi: 10.1175/MWR-D-11-00012.1

Dobricic S, Pinardi N. 2008. An oceanographic three-dimensional variational data assimilation scheme. *Ocean Modell.* **22**: 89–105, doi: 10.1016/j.ocemod.2008.01.004.

Dobricic S, Pinardi N, Adani M, Bonazzi A, Fratianni C, Tonani M. 2005. Mediterranean Forecasting System: An improved assimilation scheme for sea-level anomaly and its validation. *Q. J. R. Meteorol. Soc.* **131**: 3627–3642, doi: 10.1256/qj.05.100.

Dobricic S, Pinardi N, Adani M, Tonani M, Fratianni C, Bonazzi A, Fernandez V. 2007. Daily oceanographic analyses by Mediterranean Forecasting System at the basin scale. *Ocean Sci.* **3**: 149–157, doi: 10.5194/os-3-149-2007.

Epstein ES. 1962. A Bayesian approach to decision making in applied meteorology. *J. Appl. Meteorol.* **1**: 169–177.

Etherton BJ, Bishop CH. 2004. Resilience of hybrid ensemble/3D-Var analysis schemes to model error and ensemble covariance error. *Mon. Weather Rev.* **132**: 1065–1080.

Evensen G. 1994. Sequential data assimilation with nonlinear quasi-geostrophic model using Monte Carlo methods to forecast error statistics. *J. Geophys. Res.* **99**: 143–162, doi: 10.1029/94JC00572.

Gilks WR. 1996. Full conditional distributions. In *Markov Chain Monte Carlo in Practice*, Gilks WR, Richardson S, Spiegelhalter DJ. (eds.): 75–88. Chapman & Hall/CRC: London.

Hamill TM, Snyder C. 2000. A hybrid ensemble Kalman filter–3D variational analysis scheme. *Mon. Weather Rev.* **128**: 2905–2919.

Lermusiaux PFJ, Robinson AR. 1999. Data assimilation via error subspace statistical estimation. Part I: Theory and schemes. *Mon. Weather Rev.* **127**: 1385–1407.

Lorenc AC. 1986. Analysis methods for numerical weather prediction. *Q. J. R. Meteorol. Soc.* **112**: 1177–1194.

Madec G. 2008. *NEMO Ocean Engine*. Note du Pole de Modélisation No 27. Institut Pierre-Simon Laplace (IPSL): Paris.

Moore AM, Arango HG, Broquet G, Powell BS, Weaver AT, Zavala-Garay J. 2011. The Regional Ocean Modeling System (ROMS) four-dimensional variational data assimilation systems: Part I –System overview and formulation. *Prog. Oceanogr.* **91**: 34–49.

Oddo P, Adani M, Pinardi N, Fratianni C, Tonani M, Pettenuzzo D. 2009. A nested Atlantic–Mediterranean Sea general circulation model for operational forecasting. *Ocean Sci.* **5**: 461–473, doi: 10.5194/os-5-461-2009.

Oke PR, Brassington GB, Griffin DA, Schiller A. 2008. The Bluelink Ocean Data Assimilation System (BODAS). *Ocean Modell.* **21**: 46–70, doi: 10.1016/j.ocemod.2007.11.002.

Olsen AR. 1975. Bayesian and classical statistical methods applied to randomized weather modification experiments. *J. Appl. Meteorol.* **14**: 970–973.

Pinardi N, Coppini G. 2010. Operational oceanography in the Mediterranean Sea: The second stage of development. *Ocean Sci.* **6**: 263–267.

Pinardi N, Bonazzi A, Dobricic S, Milliff RF, Wikle CK, Berliner LM. 2011. Ocean ensemble forecasting. Part II: Mediterranean Forecast System response. *Q. J. R. Meteorol. Soc.* **137**: 879–893, doi: 10.1002/qj.816.

Poulain P-M, Barbanti R, Font J, Cruzado A, Millot C, Gertman I, Griffa A, Molcard A, Rupolo V, Le Bras S, Petit de la Villeon L. 2007. MedArgo: A drifting profiler program in the Mediterranean Sea. *Ocean Sci.* **3**: 379–395.

Robert CP, Casella G. 2004. *Monte Carlo Statistical Methods*. Springer: New York, NY.

Wang X, Hamill TM, Whitaker JS, Bishop CH. 2007. A comparison of hybrid ensemble transform Kalman filter –Optimum interpolation and ensemble square root filter analysis schemes. *Mon. Weather Rev.* **135**: 1055–1076, doi: 10.1175/MWR3307.1

Wang X, Barker DM, Snyder C, Hamill TM. 2008. A hybrid ETKF–3D Var data assimilation scheme for the WRF model. Part I: Observing system simulation experiment. *Mon. Weather Rev.* **136**: 5116–5131, doi: 10.1175/2008MWR2444.1.

Weaver AT, Vialard J, Anderson DLT. 2003. Three- and four-dimensional variational assimilation with an ocean general circulation model of the tropical Pacific Ocean. Part 1: Formulation, internal diagnostics and consistency checks. *Mon. Weather Rev.* **131**: 1360–1378.

Wikle CK, Berliner LM. 2007. A Bayesian tutorial for data assimilation. *Physica D* **230**: 1–16.

Wikle CK, Milliff RF, Herbei R, Leeds WB. 2013. Modern statistical methods in oceanography: A hierarchical perspective. *Stat. Sci.* **28**: 466–486, doi: 10.1214/13-STS436.

